ACS OMEGA

http://pubs.acs.org/journal/acsodf

Article

Universal Strategy to Efficiently Coat Zeolitic Imidazolate Frameworks onto Diverse Substrates

Xiaoqiang Zhang, Shuoshuo Yang, Ruofei Lu, Xingjie Zan,* and Na Li*

Cite This: *ACS Omega* 2022, 7, 17765−17773

Read Online

ACCESS | Metrics & More | Article Recommendations | Supporting Information

ABSTRACT: Anchoring metal−organic framework (MOF) coating has attracted extensive interest due to its wide applications in drug delivery, gas storage and separation, catalysis, and so forth. Here, we reported a flexible strategy on generating ZIF-8 coatings onto diverse substrates in the scale up to hundreds cm^2, independent of the geometry of the substrate, with controllable thickness, texture structure, and crystal size of coating. By understanding the mechanism and factors on the formation of ZIF-8 coatings, various zeolitic imidazolate framework coatings were successfully produced. This general strategy and in-depth insights pave the new highway to the design and synthesis of MOF coatings onto diverse substrates.

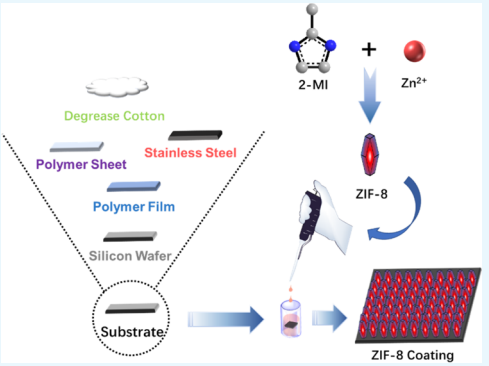

1. INTRODUCTION

Metal−organic frameworks (MOFs), constructed by metal ions as coordinative center and organic ligand as linkers,[1] have become a prominent and encouraging hotspot in the field of drug delivery, gas storage and separation, catalysis, and so forth,[2−4] relying on their exceptionally high surface areas, highly ordered molecular structure, and tunable microporosity. Anchoring MOF thin coating or membrane[5] onto materials has been demonstrated not only surmounting their limited processability in device fabrication and related applications because of the inherent rigid and fragile characteristics of MOFs but also endowing the bulk materials with non-native properties originated from MOFs and expended applications, including promoted luminescence, electronic conductivity, pollution removal, gas separation, enhanced sensitivity in sensors, and so forth.[6−9]

Numerous strategies for generating thin MOF coatings onto the supporting substrates had been developed,[10] which could be categorized into two strategies: direct and indirect. In the direct strategy, the MOF coating was in situ settled on the supporting substrates during MOF formation. Hydro-/solvothermal was the first-reported successful direct approach to grow MOF thin coatings onto the gold substrate modified by molecules with the COOH terminal group, as demonstrated by Fischer et al. in 2005.[11] Subsequently, Shekhah and co-workers reported a stepwise method of successful deposition of the HKUST-1 film onto COOH- or OH-modified substrates, in which the substrates were alternatively immersed into metal and organic precursors.[12] Ma et al. successfully prepared a continuous and defection-free MOF film onto polyacrylonitrile by preseeding 2D MOF nanosheets and following step-by-step deposition of metal ions and organic linkers.[13] Plengplung's team prepared ZIF-8 membranes on polyurethane foam substrates using a combination of seed anchoring and secondary growth, in which the substrate was modified with polyelectrolyte multilayers to enhance the initial anchoring of ZIF-8.[14] Followed by the bloom in a series of approaches, including dip-coating deposition, spin-coating deposition, electrochemical deposition, epitaxial growth, and so forth,[15−19] direct deposition of MOF coatings onto the supporting substrates has been proposed. In the indirect strategy, MOF coatings were obtained by launching the supporting substrate with the as-prepared free-standing MOF film, which was synthesized at the liquid−liquid or liquid−air interface.[20,21] Although these strategies have been successful and the enormous potential of MOF coatings has been proposed, there are several obstacles on the way to their industrial applications, for example, poor processability in hydro-/solvothermal, expensive equipments required in electrochemical deposition, time consuming in stepwise method, specific substrate designed to direct the growth of MOF crystals in epitaxial growth. A general approach to the synthesis of MOF coatings on a large scale, high-efficiency, mild conditions is still highly desired to meet the requirement for their industrial applications.

Received: February 16, 2022
Accepted: April 7, 2022
Published: May 16, 2022

https://doi.org/10.1021/acsomega.2c00939
ACS Omega 2022, 7, 17765−17773

Table 1. Applied Concentration of Metal Ions and Molar Ratios of Organic Linkers to Metal Ions to Fabricate Other ZIF Coatings

coating samples	metal ion concentration (M)	organic ligand	molar ratio (ligands/metal ions)
Co@2-methylimidazole[a]	Co^{2+}/0.06	MeIm	4:1
Cu@2-methylimidazole[a]	Cu^{2+}/0.02	MeIm	16:1
Zn@1-vinylimidazole[a]	Zn^{2+}/0.02	ViIm	8:1
Zn@aldehyde-4-imidazole[b]	Zn^{2+}/0.016	AlIm	10:1

[a]The solvent used for synthesis was water. [b]The solvent was methanol.

Compared to indirect approaches, the direct approaches are expected to receive more success because of their less step and better integration at the interface of MOF coating and the supporting substrate, especially in the case of the substrates with irregular shape. For direct synthesis, one of the biggest challenges was to grow continuous MOF coatings on inactive substrates due to the inefficient nucleation points and lack of binding sites for MOF crystals formed in mother solution.[22,23] Modifying the substrate with functional groups (such as COOH, OH, and NH_2) that is beneficial to binding metal ions or organic ligand was illustrated to enhance the generation of MOF coatings, but it is limited on the substrates with capable thiolate- or silane-chemistry. Seeking the way to endow the surface of various substrates with efficient binding sites to metal ions and/or organic ligands was significant to strengthen the nucleation, adherence of MOF crystals, and the following growth of MOF coating, which was always the endeavor.

The layer-by-layer (LBL) assembly technique discovered by Decher et al. has attracted enormous interest because of its ability to coat abundant matters onto various substrates, independent of the shapes and chemical compositions of the substrates.[24] Taking advantage of the functional groups formed by LBL coating, materials expended their applications to a wide variety of fields, including biomedicine, bioimaging, tissue engineering, separation, and so forth, as fueled by innovation in the assembly technologies and available materials.[25] Herein, we hypothesize that the functional groups provided by the LBL technique offer the nucleation and adherent sites for MOF film growth. Our data demonstrated that this strategy could be flexible on generating zeolitic imidazolate framework[26] (ZIFs, a subclass of MOFs, porous crystals with zeolite-type structures constructed by metal ions and imidazolate ligands) coatings onto the numbers of substrates [including silicon wafer (SW), stainless steel (SS), polylactic acid (PLA), polypropylene (PP), and 3d absorbent cotton], independent of the geometry of the substrates, on a large scale (up to several 10 cm), with controllable thickness (from several hundred nanometers to several micrometers).

2. EXPERIMENTAL SECTION

2.1. Materials. $Zn(NO_3)_2{\cdot}6H_2O$, $Cu(NO_3)_2{\cdot}3H_2O$, $CoCl_2{\cdot}6H_2O$, 2-methylimidazole (MeIm), 1-vinylimidazole (ViIm), aldehyde-4-imidazole (AlIm), polyacrylic acid (PAA, $M_w \sim 3k$), and polystyrene latex microsphere (PS) were purchased from Aladdin. Polyvinylphosphonic acid (PVPP), PP, $M_w \sim 250k$, PLA, polydimethyldiallyl ammonium chloride (PDDA), and tannic acid (TA) were purchased from Sigma-Aldrich. Polysodium-*p*-styrenesulfonate (PSS, wt ~ 70k) and polyallylamine hydrochloride (PAH, wt ~ 150k) were purchased from JK Chemicals. SS was purchased from a local shop. All reagents and solvents in this experiment were commercial products and used without further purification. SWs were pretreated with a piranha solution (70% H_2SO_4 and 30% H_2O_2, V/V). Caution! Piranha solution is extremely dangerous! The deionized water used in the whole process was purified through a Milli-Q system and arrived at a resistivity greater than 18.25 MΩ cm.

2.2. Pretreating of Diverse Substrates. Diverse substrates, including PLA, PP, PS, SS, and SW, were predeposited with polyelectrolyte multilayers by the LBL technique, as reported in elsewhere.[27] Briefly, these substrates were cleaned with ethanol to remove any contaminants from their surface and then were alternative-immersed into the polycation (PDDA or PAH) solution and polyanion (PAA, PSS, TA, or PVPP) until a desired number of layers (n) were reached and noted as $(\text{polycation/polyanions})_n$. Enough water was used to wash out the loosely adsorbed polyelectrolytes. The solution of all polyions was 1 mg mL^{-1} at pH 7.

2.3. Generation of the ZIF Coating on Diverse Substrates. Diverse substrates pretreated or non-pretreated with polyelectrolyte multilayers were horizontally lied down on an artificial holder, which was set in a container. The 0.01 M $Zn(NO_3)_2$ and MeIm solutions (with the molar ratio of Zn^{2+} to MeIm fixed at 1:10) were sequentially injected into the container. The injected solutions had to fully cover the substrates. After injecting $Zn(NO_3)_2$ and MeIm, the solution was sonicated for 20 s to ensure that these solutions were totally mixed. The container was set into a water bath with the reaction temperature controlled at 25 °C. After overnight, the substrate was taken out and washed thoroughly, and the side beneath the substrate was used for all characterizations to avoid the interference of the precipitation of big crystals in solution onto the top side.

During the study on the growth mechanism of Zn@2-methylimidazole (ZIF-8) coating, the substrates were taken out at the preset time points: 2, 6, and 16 h for observation.

2.4. Factors on ZIF Coating Generation. The SW predeposited with $(PDDA/TA)_3$ was used for these investigations, and the generation of ZIF coating was performed in the above section. For the temperature effect on ZIF coating generation, the temperatures were set as 25, 40, and 60 °C, which were controlled by a water bath, and all reactants were preheated at preset temperatures. For the molar ratio of MeIm to Zn^{2+}, the ratios were set at 4:1, 6:1, 8:1, and 16:1, with a fixed $Zn(NO_3)_2$ concentration at 0.01 M. For an increased $Zn(NO_3)_2$ concentration at 0.02 M, the molar ratio of MeIm to Zn^{2+} was 10:1. For investigating the effect of numbers of repeating cycles on the thickness of the ZIF coating, the substrate was taken out and washed thoroughly to remove the loosely attached ZIF precursors or crystals before repeating the ZIF coating procedure.

2.5. Generation of Other ZIF Coatings. The SW predeposited with $(PDDA/TA)_3$ was used for these investigations, and the protocols on generating other ZIF coatings were the same as the growth of ZIF-8 coating. Cu^{2+} and Co^{2+} were chosen instead of Zn^{2+}, and AlIm and ViIm were used instead of MeIm. The concentration of metal ions and the molar ratio of organic linkers to metal ions are listed in Table 1, and the reaction temperature was 25 °C.

https://doi.org/10.1021/acsomega.2c00939
ACS Omega 2022, 7, 17765−17773

Scheme 1. Molecular Structures of (a) TA and (b) PDDA and (c) Schematic Illustration on the Strategy for ZIF Coatings onto the Numbers of Substrates[a]

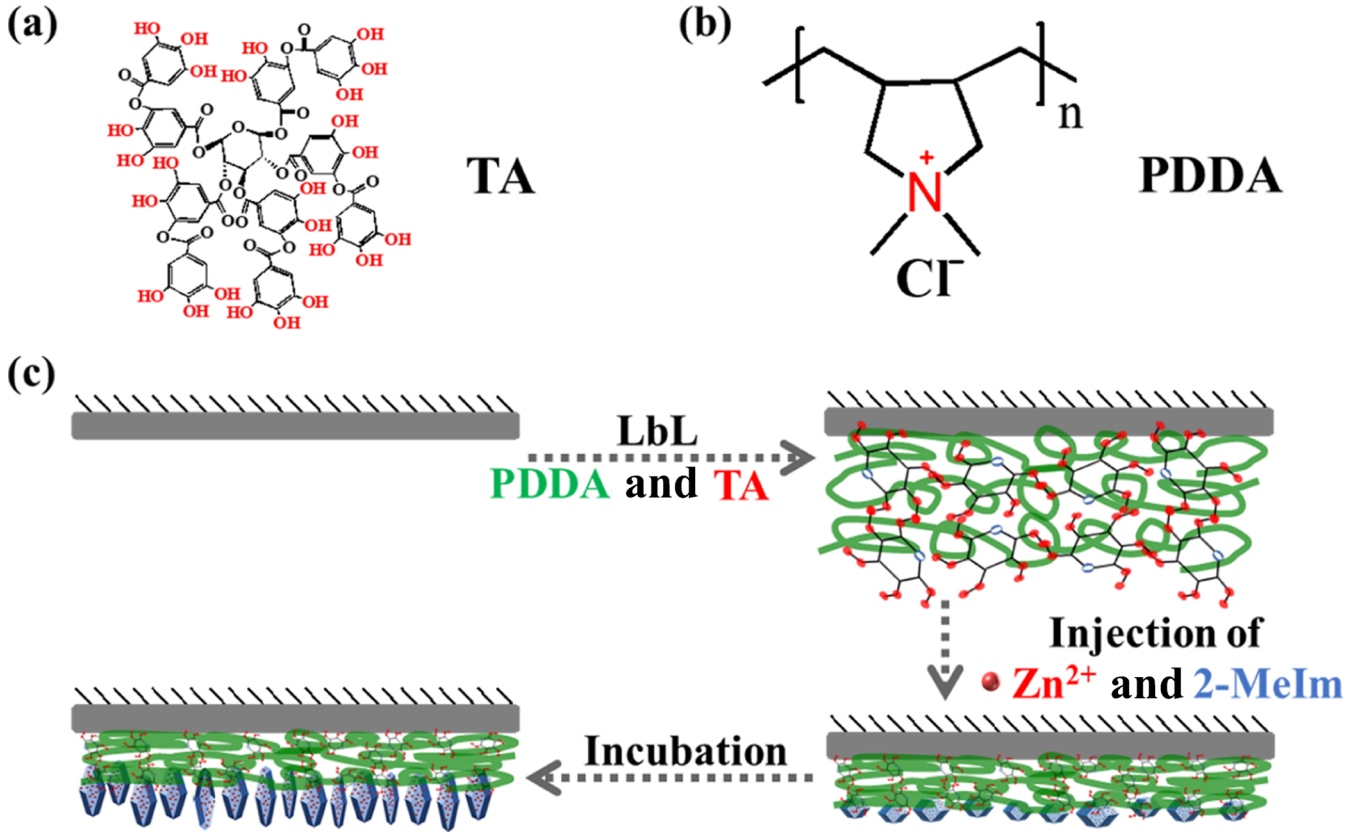

[a]The substrates were pretreated with polyelectrolyte multilayers PDDA and TA and then were horizontally lied down on an artificial holder, which was set in a container. $Zn(NO_3)_2$ and 2-MeIm solutions were sequentially injected into the container until the solutions had fully covered the substrates. After the desired incubation time, the substrate was washed thoroughly for all characterizations to avoid the interference of the precipitation of large crystals in solutions falling onto the top side.

2.6. Characterization. Scanning electron microscopy (SEM) for the surface morphological analysis was carried out on a SU8010 SEM using the SE (L) measuring mode with an acceleration voltage of 3 kV and a working current of 10 μA. Sputter-coated Pt was used for the coating additional conductivity. The powder X-ray diffraction (XRD) patterns of samples were acquired with a Rigaku XDS 2000 diffractometer (Cu Kα_1 radiation) with the transmission mode. Water contact angle (WCA) analyses were carried out using the static sessile drop method with water as the probe liquid on a KRUSS DSA1 version 1.80 drop shape analyzer. The reported contact angle value was an average of at least 10 measurements. The powder samples were processed by blending and grinding with KBr and then pressed to form the pellets. Attenuated total reflection (ATR)−Fourier transform infrared (FTIR) spectra were recorded in the wavenumber range of 400−1750 cm^{-1} on a Tensor II spectrometer (Bruker ALPHA II, Germany) on the ATR mode. A complete set of studies pertinent to elements of ZIF coatings (C, N, and Zn) were further performed on a Vario El cube energy-dispersive spectroscope at a voltage of 3.0 kV for 30 min. The digital pictures were taken with the SONY (NEX-6) camera.

3. RESULTS AND DISCUSSION

3.1. Fabrication of the ZIF-8 Coating on Diverse Substrates on a Large Scale. As illustrated in Scheme 1, the ZIF coatings were straightforwardly generated on a SW pretreated with a LBL film of $(PDDA/TA)_3$ by sequentially injecting metal ions (Zn^{2+}) and organic ligands (MeIm) into a container to immerse the silicon substrate. After the desired incubation time (24 h, enough for MOF coating growth), the SW was thoroughly washed and dried. To show the potency of this strategy on the generation of MOF coatings on a large scale, the manually cut SW with a scale of ∼15 cm × 12 cm was selected for demonstration. Before and after the MOF coating, images of the SWs were taken and are shown in Figure 1a, where a macroscopic white film (Figure 1a, bottom) was evenly coated compared to the dark before the MOF coating (Figure 1a, top). The WCA, a technique sensitive to surface changes, shifted from 21 to 132° (Figure S1), which proved the successful generation of coating. Under the magnified image at the edge or the center of the SW, the coating was very uniform and continuous without any obvious pinholes, cracks, or other defects (Figure 1b). With further magnification, a lawn-like, well-intergrown micro−nanostructure was observed (Figure 1c). More interestingly, the arrangement of "grass" showed a certain orientation, indicating that our coating had a certain orientation. Obviously, the SEM cross-sectional image (Figure 1d) further supported the uniform and continuous coating. The magnified image (Figure 1e) suggested that the coating was firmly attached to the beneath substrate, with an approximate thickness of 1.8 μm. During the formation of coating, the solution became turbid, suggesting that the particles were generated in the solution.

https://doi.org/10.1021/acsomega.2c00939
ACS Omega 2022, 7, 17765−17773

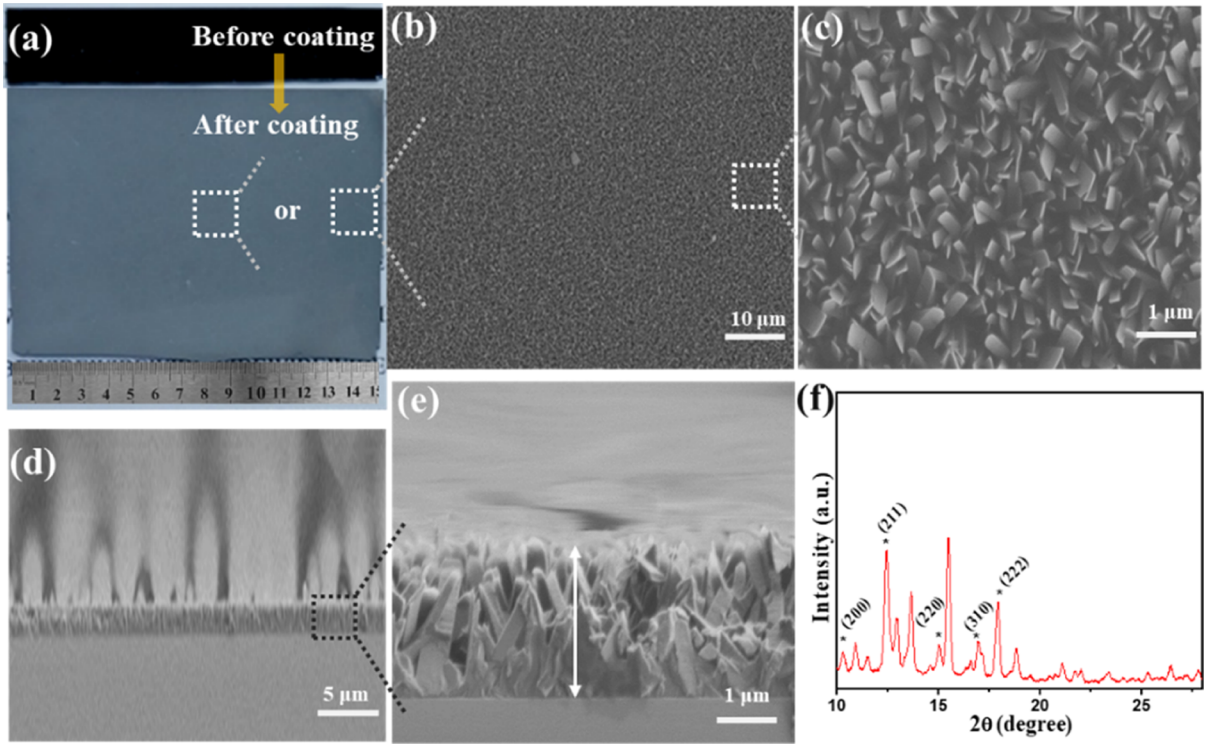

Figure 1. (a) Digital photograph of ZIF-8 coatings on SW; (b−e) SEM images of ZIF-8 coatings on the SW substrate; and (f) XRD spectra of ZIF-8 coatings on the SW substrate.

These particles were pinned down and freeze-dried to a powder for further analysis by SEM and XRD. In addition to the typical morphology of ZIF-8 particles, a regular dodecahedron structure was found by the SEM characterization of ZIF-8 powders (Figure S2a). The crystalline structure of the formed coatings was conducted by XRD and displayed in Figure 1f. Some characteristic diffraction peaks designed to ZIF-8, including (200), (211), (220), (310), and (222) at 10.9, 12.4, 14.8, 16.8, and 17.9 degree, respectively, were clearly observed, which was consistent with previous reports.[28] In the diffraction pattern of the powder obtained from the solution (Figure S2b), these characteristic diffraction peaks could be observed as well. The totally different relative intensities of these peaks between the coating and powder reflected the orientation of crystals on coating, which was in line with the SEM observation (Figure 1c). Other unassigned peaks at 15.6, 18.9, and 21.1 degrees in Figures 1f and S2b might be attributed to the impurities. Meanwhile, in the FTIR spectra (Figure S3), the peaks at 1568 and 433 cm^{-1} were assigned to C═N stretching and Zn−N, respectively, which were in good correspondence with the characteristic peak of ZIF-8 in a previous study.[29] In addition, as can be seen from energy-dispersive spectroscopy (EDS) measurements (Figure S4a−d), the elements of ZIF-8 coatings mainly included C, N, and Zn, and the signal of silica totally disappeared. All these data identified that the generated coating was ZIF-8.

On the basis of successful preparation of ZIF-8 coatings on the SW substrate, we further explored whether this strategy has universal applicability on various substrates. The representative among metal materials, steel sheets (SS), and a series of representative plastic films including PLA, PP, and PS was conscripted. After the deposition of $(PDDA/TA)_3$ on these substrates by LBL, ZIF-8 coatings seemed to be successfully grown, as demonstrated by a digital camera (Figure 2a). The

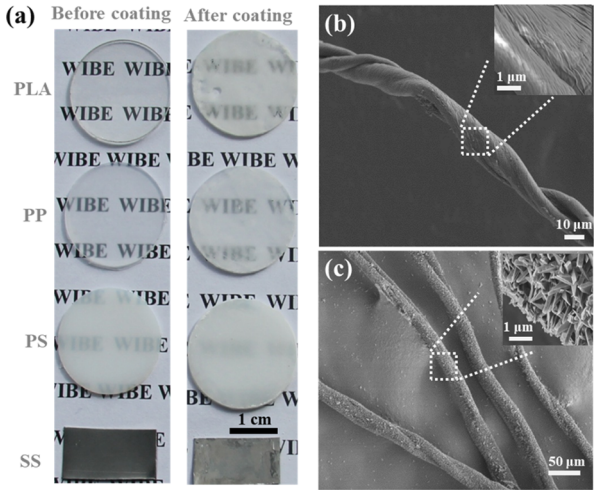

Figure 2. (a) Digital photograph of the ZIF-8 coating on PLA, PP, PS, and SS substrates coated with $(PDDA/TA)_3$ and their control and (b,c) SEM image (b) before and (c) after the coating on degrease cotton and the corresponding high-magnification SEM images (insets).

WCAs of these substrates after the ZIF-8 coating were very close to each other, falling into a narrow range of 125−135° (Figure S1), indicating the successful ZIF-8 coating growth. In addition, the SEM micrographs (Figure S5) revealed the obvious similarities of the micro- and nanomorphology of the ZIF-8 coatings on SW treated by this strategy. It was basically determined that the strategy had a suitable adaptability to 2D substrates. Next, whether this strategy could be used on 3D substrates was explored. Degrease cotton was selected to be a typical representative of 3D substrates because of its fiber structure. Figure 2b, andFigure 2c presented the SEM image before and after the coating on the fibers of degrease cotton. The

https://doi.org/10.1021/acsomega.2c00939
ACS Omega 2022, 7, 17765−17773

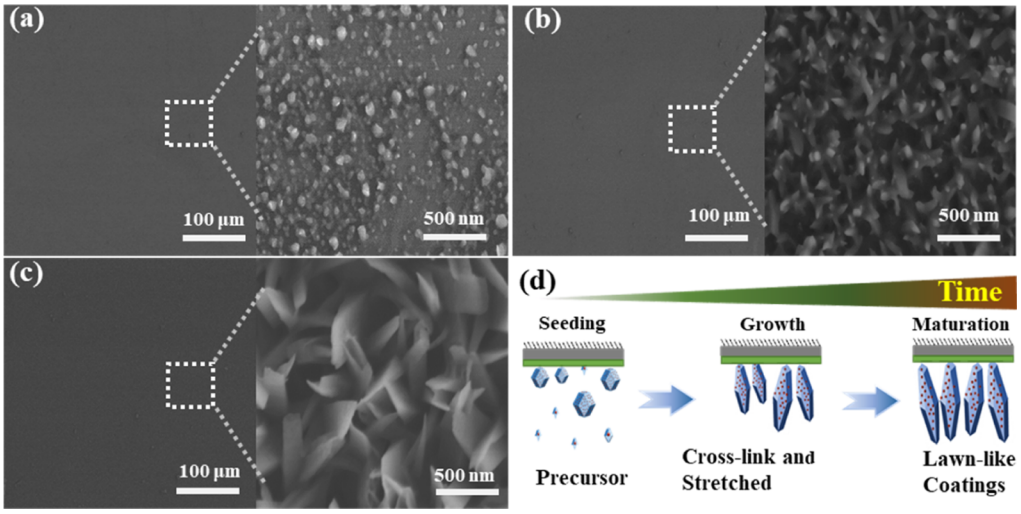

Figure 3. (a−c) SEM images of the growth process of ZIF-8 coatings at (a) 2, (b) 4, and (c) 16 h and (d) cartoons illustrating the growth process of ZIF-8 coatings with increased incubation time. The right panel in each figure shows the magnified image in the square of the left panel.

degrease cotton fibers before the coating appeared a relatively smooth surface (Figure 2b), and the seemingly prickly surfaces (Figure 2c) were observed on degrease cotton fibers after the coating. In the high-magnification SEM images, the continuous and uniform coatings with a similar micro- and nanomorphology of the ZIF-8 coatings to that grown on 2D substrates were observed after coating formation (insets of Figure 2c), compared with a smooth surface of degrease cotton fibers before the coating (insets of Figure 2b). These results demonstrated that a simple and potent strategy had been proposed to successfully synthesize a continuous, flawless, well-oriented ZIF-8 coating on the diverse substrates on a large scale, independent of the geometry, dimensions, and chemical compositions of substrates.

3.2. Factors and Growth Mechanisms. With the mind of understanding the growth mechanism, factors on the growth of ZIF-8 coatings onto diverse substrates were investigated. As a control, the diverse substrates (PLA, PP, PS, and SS) without the deposition of polyelectrolyte multilayers were used for the growth of ZIF-8 coatings. Although the growth of ZIF-8 coatings on plastics (PLA, PP, and PS) could also be found in their SEM images (Figure S6a−c), uncovered areas were clearly observed in the magnified images (insets in Figure S6a−c). For the SS or silicon substrate, although the coverage of ZIF-8 coatings was much higher than that on plastics (Figure S6d and the inset in Figure S6d), the density was much lower than that on the SS or silicon substrate pretreated by $(PDDA/TA)_3$ (Figures 1c and S5d). Besides, the growth of ZIF-8 coatings was slightly dependent on the layer numbers of the deposited polyelectrolyte, as supported by the SEM images in Figure S7a−h. The growth of ZIF-8 coatings on all substrates (PLA, PP, PS, and SS) treated by single PDDA and $(PDDA/TA)_{3.5}$ layers was successful, but the density of ZIF-8 on substrates treated by single PDDA seemed slightly lower than those pretreated by $(PDDA/TA)_{3.5}$. These results suggested that the deposition of polyelectrolyte multilayers was the key factor in the growth of ZIF-8 coatings.

As known, there have been plentiful reported materials to build the multilayer coatings, and the property of the coating was dominated by the outmost layer. To further amplify the feasibility of this strategy, a variety of representative assemble pairs were recruited, including PAH/PAA, PDDA/PSS, and TA/PVPON, to pretreat the PS substrate (on which the ZIF-8 coating was hard to directly grow) with different outmost layers. Another reason for selecting these assemble pairs and treating the substrate with different outmost layers was the purpose of investigating the effect of these functional groups brought with the deposition of the outmost layer on the growth of ZIF-8 coatings. Here, based on their molecular structures demonstrated in Scheme 1a,b and Figure S8a−d, the terminals of PAA, PAH, PSS, PDDA, PVPON, and TA were expected to endow the surface with −COOH, $-NH_2$, $-SO_3-$, $-{}^+NR_4$, −CO−NH−, and ph-OH. The SEM images (Figure S9a−f) showed that the continuous ZIF-8 coatings were successfully acquired on the PS substrate treated by these polyelectrolytes, suggesting that this strategy has good applicability for various functional groups. Noteworthily, a more important fact was that the growth morphologies of the coatings on various polyelectrolyte-treated substrates with different terminated functional groups were extremely similar. It is roughly concluded that the ZIF-8 coatings were almost not affected by the functional groups of the underlying substrates and had universal applicability to substrates pretreated by a variety of polyelectrolytes.

To better understand the formation of ZIF-8 coatings, the morphological characteristics during the growth process were observed. When the mixture of MeIm and $Zn(NO_3)_2$ was brought in contact with the substrate for 2 h, granular crystals with an average size of 1−100 nm (Figure 3a) were produced on the surface of the substrate. Extending the contact time to 4 h, the original crystal particles gradually cross-link the growth and stretch toward different directions (Figure 3b). Subsequently, an interlaced lawn-similar structure with a size of 100−500 nm was formed when reacted for 16 h, accompanied with the successful preparation of a lawn-like ZIF-8 coating (Figure 3c). Gathering these data, it is reasonable to speculate that the ZIF-8 coatings were generated through at least three stages: seeding of the ZIF-8 precursor and growth and maturation of the ZIF-8 coating (Figure 3d).

At the beginning stage, the ZIF-8 precursor generated from the enriched metal ions and ligands near the surface of the substrate or directly deposited from the mother solution started seeding onto the substrate. The seeded precursor acted as the crystal growth site, and the growth of the ZIF-8 coating was fueled by the precursor in the mother solution until run out. As the ZIF-8 coating grows, the ZIF-8 crystals had to grow vertically

https://doi.org/10.1021/acsomega.2c00939
ACS Omega 2022, 7, 17765−17773

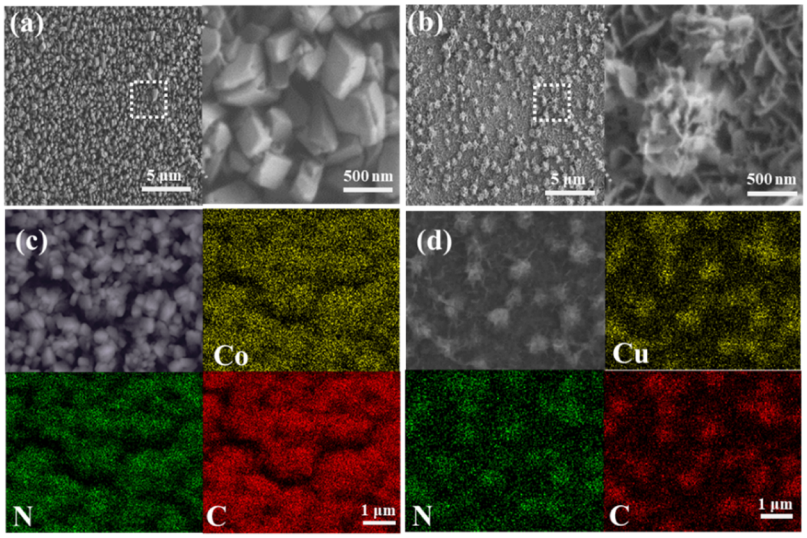

Figure 4. (a,b) SEM images of (a) Co@2-methylimidazole and (b) Cu@2-methylimidazole. The right panel in each figure shows the magnified image in the square of the left panel. (c,d) EDS mapping of (c) Co@2-methylimidazole and (d) Cu@2-methylimidazole coatings.

due to the confined space, forming an interlaced structure. Obviously, the binding ability of the substrate to precursors was critical to heterogeneous nucleation of ZIF-8, and the seeding density was determinant of the following density of ZIF-8 crystals. Compared to the native plastic film, the multilayer-pretreated plastic had stronger binding ability to precursors due to the presence of functional groups (−COOH, $-NH_2$, $-SO_3^-$, $-^+NR_4$, −CO−NH−, and ph-OH) from the deposited material, which lead to a high density of ZIF-8 coatings. This is the reason for the differences in the density of ZIF-8 coatings on diverse substrates.

In the coating growth stage, the way to supply precursors was significant to the coating thickness and coating morphology. To further prove the growth mechanism, precursors produced at varied conditions were fed for the growth of the ZIF-8 coating, which are expected to produce different ZIF-8 coatings. As demonstrated in Figure S10, on the premise of keeping the concentration of Zn^{2+} at 0.01 M, the morphology of the ZIF-8 coating evolved vastly with the molar ratio of 2-MeIm to Zn^{2+} varying from 4:1 to 16:1. At a low proportion of 2-MeIm (2-MeIm toZn^{2+}, 4:1) (Figure S10a), the polyhedron particles scattered onto the substrate were hard to fully cover the substrate. Until the molar ratio of 2-MeIm to Zn^{2+} increased higher than 8:1, the substrate was fully covered with a similar micro- and nanomorphology of the ZIF-8 coating (Figure S10b−d). Although these coatings exhibited similarity on the surface texture, the detailed analysis revealed the increased crystal width from about 400 nm (Figure S10b) to 1.3 μm (Figure S10d). On the other hand, although the molar ratio of 2-MeIm to Zn^{2+} remained 10:1, the morphology and shape of the prepared coatings significantly changed, while the concentration of Zn^{2+} varied from 0.01 to 0.02 M, which is evidenced by the ZIF-8 coating's corresponding SEM images (Figure 1c vs S10e).

Temperature was another key factor in controlling ZIF-8 formation. It has been reported that the growth rate and size of crystal nucleus are strongly sensitive to temperature alterations.[30] With increasing temperature from 25 to 60 °C, the morphology of the ZIF-8 coating evolved from a single leaf-like crystal (Figure 1c at 25 °C and Figure S11a at 40 °C) to a laminar aggregated crystal (Figure S11b at 60 °C). Interestingly, the thickness increased from 1.8 μm at 25 °C to 3.2 μm at 40 °C and 4.2 μm at 60 °C. Considering that the growth of the ZIF-8 coatings was sustained from the deposition of precursors in the mother solution and stagnated when the precursors run out, replenishment of precursors should further increase the coating thickness. Figure S12a−d shows the cross-section of the ZIF-8 coating fabricated by repeating the ZIF coating process, and the thickness was strongly dependent on the numbers of repeating cycles, increasing from 1.8 μm 1st cycle to 3.5 μm at 2nd cycle and 5.3 μm at 3rd cycle. It has to be mentioned that the texture structure of ZIF-8 coatings actually changed at a certain degree, from a compact and tightly interlaced lawn-like structure to a loose and fluffy irregular structure. All these results revealed that the variation of the synthesis conditions (concentration, molar ratio, temperature, and numbers of repeating cycles) significantly affected the morphology and thickness of the ZIF-8 coating, which also offered an effective way to control the thickness, texture structure, and crystal size of the ZIF-8 coating.

The beginning stage was critical to the following growth stage. The basic mechanism of the enhanced growth of the ZIF-8 coating on the polyelectrolyte multilayer-modified substrate was mainly due to the multiple interactions between the predeposited polyelectrolytes and metal ions and the organic linker, including coordinative interaction, hydrogen bonding, electrostatic interactions, and so forth. Such multi-interactions were present between predeposited polyelectrolytes and the precursors in solution as well. Overall, the presence of the deposited polyelectrolyte provided the affinity to precursors, enriched metal ions, and ligands near the surface of the substrate or directly deposited from the mother solution. Then, the deposition and formation of nucleation in the solution dominated the following growth stage, which was influenced by the temperature and feeding ratio between metal ions and organic linkers.[31,32] Obviously, any factors on adjusting these multi-interactions and nucleation process could contribute to the formation of MOF coatings.

3.3. Growth of Other ZIF Coatings. We speculated that the construction of ZIF-8 coatings had facilitated the process of design and had set necessary conditions for the synthesis of other coatings, and the strategy can also be extended to relevant ZIF coatings. ZIFs are composed of bivalent metal ions and bridging substitutional imidazolate ligands, whose features are

https://doi.org/10.1021/acsomega.2c00939
ACS Omega 2022, 7, 17765−17773

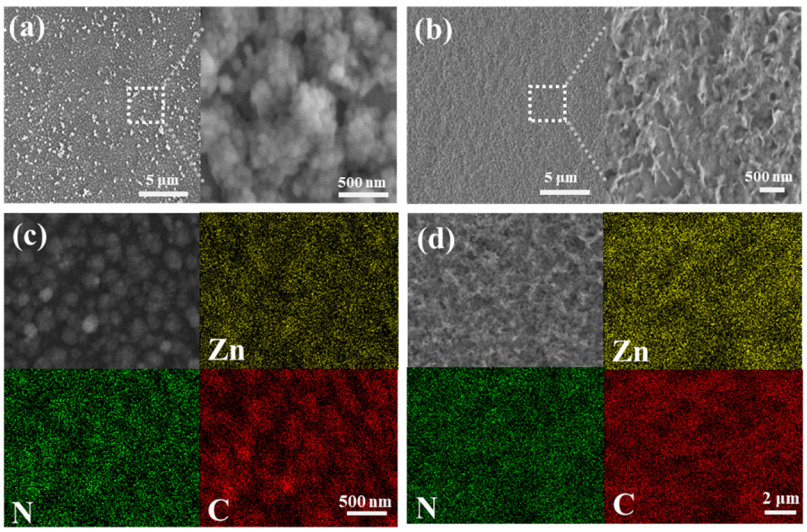

Figure 5. (a,b) SEM images of (a) Zn@1-vinylimidazole and (b) Zn@aldehyde-4-imidazole coatings. The right panel in each figure shows the magnified image in the square of the left panel. (c,d) EDS mapping of (c) Zn@1-vinylimidazole and (d) Zn@aldehyde-4-imidazole coatings.

akin to traditional inorganic zeolites topology. Based on the ligands of ZIFs, it has been reported that the thermal and chemical stability could be largely improved.[21] In the following, we tried to verify the feasibility of the experimental strategy by changing the metal ions and organic ligands for the preparation of other ZIFs.[33] Cu^{2+}, Co^{2+} instead of Zn^{2+}, AlIm and ViIm instead of the organic linker MeIm were chosen to verify our conjecture.

In the case of Co@2-MeIm coatings (Figure 4a), as can be seen in the SEM images, the continuous, consistent coatings possess a similar micro- or nanostructure to that of ZIF-8 coatings, possibly because Zn^{2+} and Co^{2+} were similar elements both in the transition metal region of the periodic table and with the same valence state. Moreover, as indicated by the EDS results, the constituent elements of the coatings were mainly Co, C, and N (Figure 4c). When the metal ion was replaced with Cu^{2+}, as shown in Figure 4b, Cu@2-MeIm coatings were assembled cleverly alternately by the lamellar structure. The EDS results (Figure 4d) showed that the constituent elements of the Cu@2-MeIm coatings were Cu, C, and N.

Similarly, we also tried to synthesize coatings with other derivatives of imidazole. Zn^{2+} was used as the central ion, and ViIm was used as the ligand, and the coatings were prepared in the same way. The Zn@1-vinylimidazole coatings were accumulated by spherical crystal grains, and the size of individual spherical crystal grains was about 30 nm (Figure 5a). EDS results (Figure 5c) showed the constituent elements of the Zn@1-vinylimidazole coatings were Zn, C, and N. Compared to Zn@1-vinylimidazole coatings, Zn@aldehyde-4-imidazole coatings (Figure 5b) were formed by irregular lamellar accumulation, and EDS results (Figure 5d) revealed the presence of elements of C, N, and Zn. Obviously, this synthesis method was also applicable to other ZIF coatings. Therefore, this present general strategy and in-depth insights provide good directions for the design and synthesis of uniform MOF coatings independent of substrates.

4. CONCLUSIONS

In summary, a simple and potent strategy had been proposed to successfully synthesize continuous, flawless, well-oriented ZIF-8 coatings on the diverse substrates on a large scale, independent of the geometry, dimensions, and chemical compositions of substrates. Deposition of polyelectrolyte multilayers was the key factor in the growth of ZIF-8 coatings; meanwhile, the variation of the synthesis conditions (concentration, molar ratio, temperature, and numbers of repeating cycles) also affected significantly the morphology and thickness of the coating. This present general strategy and in-depth insights provide good directions for the design and synthesis of uniform MOF coatings independent of the substrates and offer an effective way to control the thickness, texture structure, and crystal size of the coating.

■ ASSOCIATED CONTENT

Supporting Information

The Supporting Information is available free of charge at https://pubs.acs.org/doi/10.1021/acsomega.2c00939.

WCA of SW surfaces with or without modification; SEM image and XRD spectra of the powder obtained from the turbid solution; FTIR spectra of the ZIF coating; EDS elemental mappings of Zn, N, and C in the ZIF-8 coatings; diagram of the total element content of ZIF-8 coatings; SEM images of ZIF-8 coatings on PLA, PP, PS, and SS substrates coated with $(PDDA/TA)_3$; SEM images of ZIF-8 coatings on PLA, PP, PS, and SS or silicon substrates without the $(PDDA/TA)_3$ coating; SEM images of ZIF-8 coatings on PLA, PP, PS, and SS substrates treated by single PDDA and multi-$(PDDA/TA)_{3.5}$ layers; molecular structures of PAH, PAA, PSS, and PVPON; SEM images of ZIF-8 coatings on the PS substrate treated by polyelectrolytes with PAH, PAA, PDDA, PSS, TA, and PVPON for the outmost layer; SEM surface images of the ZIF-8 coating on SW substrates modified by $(PDDA-TA)_3$ prepared with different mole ratios of 2-MeIm to Zn^{2+} and reactant concentrations: 4:1, 6:1, 8:1, and 16:1, $[Zn^{2+}] = 0.01$ M), 10:1, $[Zn^{2+}] = 0.02$ M; SEM images of ZIF-8 coatings generated at temperatures 40 and 60 °C and thickness of ZIF-8 coatings as a function of fabricated temperature (25, 40, and 60°C); insets in (c) show the cross-sectional SEM images of ZIF-8 coatings at the corresponding temperature; and SEM cross-sectional images of ZIF-8 coatings

https://doi.org/10.1021/acsomega.2c00939
ACS Omega 2022, 7, 17765−17773

repeated the first, second, third cycles and thickness of ZIF-8 coatings as a function of the number of repeating cycles (PDF)

AUTHOR INFORMATION

Corresponding Authors

Xingjie Zan − *Xinjiang Technical Institute of Physics and Chemistry, Chinese Academy of Sciences, Urumqi 830011, China; Oujiang Laboratory, Wenzhou Key Laboratory of Perioperative Medicine, Wenzhou Institute, University of Chinese Academy of Sciences, Wenzhou 325001, China;* orcid.org/0000-0002-0492-2913; Email: xjzan2000@hotmail.com

Na Li − *Oujiang Laboratory, Wenzhou Key Laboratory of Perioperative Medicine, Wenzhou Institute, University of Chinese Academy of Sciences, Wenzhou 325001, China;* orcid.org/0000-0002-4483-4467; Email: lina0701@ucas.ac.cn

Authors

Xiaoqiang Zhang − *Xinjiang Technical Institute of Physics and Chemistry, Chinese Academy of Sciences, Urumqi 830011, China; University of Chinese Academy of Sciences, Beijing 100049, China*

Shuoshuo Yang − *Oujiang Laboratory, Wenzhou Key Laboratory of Perioperative Medicine, Wenzhou Institute, University of Chinese Academy of Sciences, Wenzhou 325001, China; Hubei Key Laboratory of Bioinorganic Chemistry & Materia Medica, Huazhong University of Science & Technology, Wuhan 430074, China*

Ruofei Lu − *Xinjiang Technical Institute of Physics and Chemistry, Chinese Academy of Sciences, Urumqi 830011, China; University of Chinese Academy of Sciences, Beijing 100049, China*

Complete contact information is available at: https://pubs.acs.org/10.1021/acsomega.2c00939

Notes

The authors declare no competing financial interest.

ACKNOWLEDGMENTS

This work was supported by Wenzhou Key Laboratory of perioperative medicine (2021HZSY0069), the One Thousand Talents Program, and the startup funding from the Wenzhou Institute of University of Chinese Academy of Sciences (WIUCASQD2019009 and WIUCASQD2021032).

REFERENCES

(1) Furukawa, H.; Cordova, K. E.; O'Keeffe, M.; Yaghi, O. M. The Chemistry and Applications of Metal-Organic Frameworks. *Science* **2013**, *341*, 1230444.

(2) Zheng, H.; Zhang, Y.; Liu, L.; Wan, W.; Guo, P.; Nyström, A. M.; Zou, X. One-pot Synthesis of Metal−Organic Frameworks with Encapsulated Target Molecules and Their Applications for Controlled Drug Delivery. *J. Am. Chem. Soc.* **2016**, *138*, 962−968.

(3) Liu, J.; Chen, L.; Cui, H.; Zhang, J.; Zhang, L.; Su, C.-Y. Applications of metal−organic frameworks in heterogeneous supramolecular catalysis. *Chem. Soc. Rev.* **2014**, *43*, 6011−6061.

(4) Li, J.-R.; Kuppler, R. J.; Zhou, H.-C. Selective gas adsorption and separation in metal−organic frameworks. *Chem. Soc. Rev.* **2009**, *38*, 1477−1504.

(5) Shekhah, O.; Liu, J.; Fischer, R. A.; Wöll, C. MOF thin films: existing and future applications. *Chem. Soc. Rev.* **2011**, *40*, 1081−1106.

(6) Xiao, Y.-H.; Gu, Z.-G.; Zhang, J. Surface-coordinated metal−organic framework thin films (SURMOFs) for electrocatalytic applications. *Nanoscale* **2020**, *12*, 12712−12730.

(7) Qin, X.; Zhang, X.; Wang, M.; Dong, Y.; Liu, J.; Zhu, Z.; Li, M.; Yang, D.; Shao, Y. Fabrication of Tris(bipyridine)ruthenium(II)-Functionalized Metal−Organic Framework Thin Films by Electrochemically Assisted Self-Assembly Technique for Electrochemiluminescent Immunoassay. *Anal. Chem.* **2018**, *90*, 11622−11628.

(8) Klyatskaya, S.; Kanj, A. B.; Molina-Jirón, C.; Heidrich, S.; Velasco, L.; Natzeck, C.; Gliemann, H.; Heissler, S.; Weidler, P.; Wenzel, W.; Bufon, C. C. B.; Heinke, L.; Wöll, C.; Ruben, M. Conductive Metal−Organic Framework Thin Film Hybrids by Electropolymerization of Monosubstituted Acetylenes. *ACS Appl. Mater. Interfaces* **2020**, *12*, 30972−30979.

(9) Ma, X.; Chai, Y.; Li, P.; Wang, B. Metal−Organic Framework Films and Their Potential Applications in Environmental Pollution Control. *Acc. Chem. Res.* **2019**, *52*, 1461−1470.

(10) Crivello, C.; Sevim, S.; Graniel, O.; Franco, C.; Pané, S.; Puigmartí-Luis, J.; Muñoz-Rojas, D. Advanced technologies for the fabrication of MOF thin films. *Mater. Horiz.* **2021**, *8*, 168−178.

(11) Hermes, S.; Schröder, F.; Chelmowski, R.; Wöll, C.; Fischer, R. A. Selective Nucleation and Growth of Metal−Organic Open Framework Thin Films on Patterned COOH/CF3-Terminated Self-Assembled Monolayers on Au(111). *J. Am. Chem. Soc.* **2005**, *127*, 13744−13745.

(12) Shekhah, O.; Wang, H.; Kowarik, S.; Schreiber, F.; Paulus, M.; Tolan, M.; Sternemann, C.; Evers, F.; Zacher, D.; Fischer, R. A.; Wöll, C. Step-by-Step Route for the Synthesis of Metal−Organic Frameworks. *J. Am. Chem. Soc.* **2007**, *129*, 15118−15119.

(13) Ma, Y.; Dong, Z.; You, M.; Zhang, Y.; Feng, X.; Ma, X.; Meng, J. Formation of a thin and continuous MOF membrane with 2-D MOF nanosheets as seeds via layer-by-layer growth. *Chem. Commun.* **2019**, *55*, 10146−10149.

(14) Plengplung, P.-s.; Ratanatawanate, C.; Dubas, S. T. Improved stability of zeolitic imidazolate framework-8 photocatalytic coating on polyurethane foam via polyelectrolyte multilayer surface modification. *Colloids Surf., A* **2021**, *629*, 127415.

(15) Monforte, F.; Mannino, G.; Alberti, A.; Smecca, E.; Italia, M.; Motta, A.; Tudisco, C.; Condorelli, G. G. Heterogeneous growth of continuous ZIF-8 films on low-temperature amorphous silicon. *Appl. Surf. Sci.* **2019**, *473*, 182−189.

(16) Gu, Z.-G.; Fu, H.; Neumann, T.; Xu, Z.-X.; Fu, W.-Q.; Wenzel, W.; Zhang, L.; Zhang, J.; Wöll, C. Chiral Porous Metacrystals: Employing Liquid-Phase Epitaxy to Assemble Enantiopure Metal−Organic Nanoclusters into Molecular Framework Pores. *ACS Nano* **2016**, *10*, 977−983.

(17) Chaudhari, A. K.; Han, I.; Tan, J.-C. Multifunctional Supramolecular Hybrid Materials Constructed from Hierarchical Self-Ordering of In Situ Generated Metal-Organic Framework (MOF) Nanoparticles. *Adv. Mater.* **2015**, *27*, 4438−4446.

(18) Jia, Z.; Hao, S.; Wen, J.; Li, S.; Peng, W.; Huang, R.; Xu, X. Electrochemical fabrication of metal-organic frameworks membranes and films: A review. *Microporous Mesoporous Mater.* **2020**, *305*, 110322.

(19) Schoedel, A.; Scherb, C.; Bein, T. Oriented Nanoscale Films of Metal-Organic Frameworks By Room-Temperature Gel-Layer Synthesis. *Angew. Chem., Int. Ed.* **2010**, *49*, 7225−7228.

(20) Katayama, Y.; Kalaj, M.; Barcus, K. S.; Cohen, S. M. Self-Assembly of Metal−Organic Framework (MOF) Nanoparticle Monolayers and Free-Standing Multilayers. *J. Am. Chem. Soc.* **2019**, *141*, 20000−20003.

(21) Bai, X.-j.; Chen, D.; Li, L.-l.; Shao, L.; He, W.-x.; Chen, H.; Li, Y.-n.; Zhang, X.-m.; Zhang, L.-y.; Wang, T.-q.; Fu, Y.; Qi, W. Fabrication of MOF Thin Films at Miscible Liquid Liquid Interface by Spray Method. *ACS Appl. Mater. Interfaces* **2018**, *10*, 25960−25966.

(22) Van Vleet, M. J.; Weng, T.; Li, X.; Schmidt, J. R. In Situ, Time-Resolved, and Mechanistic Studies of Metal−Organic Framework Nucleation and Growth. *Chem. Rev.* **2018**, *118*, 3681−3721.

(23) Liu, J.; Wöll, C. Surface-supported metal−organic framework thin films: fabrication methods, applications, and challenges. *Chem. Soc. Rev.* **2017**, *46*, 5730−5770.

(24) Decher, G.; Hong, J. D.; Schmitt, J. Buildup of Ultrathin Multilayer Films by a Self-Assembly Process: II. Consecutive Adsorption of Anionic and Cationic Bipolar Amphiphiles and Polyelectrolytes on Charged Surfaces. *Thin Solid Films* **1992**, *210*−*211*, 831−835.
(25) Richardson, J. J.; Cui, J.; Björnmalm, M.; Braunger, J. A.; Ejima, H.; Caruso, F. Innovation in Layer-by-Layer Assembly. *Chem. Rev.* **2016**, *116*, 14828−14867.
(26) Kaneti, Y. V.; Dutta, S.; Hossain, M. S. A.; Shiddiky, M. J. A.; Tung, K. L.; Shieh, F. K.; Tsung, C. K.; Wu, K. C. W.; Yamauchi, Y. Strategies for Improving the Functionality of Zeolitic Imidazolate Frameworks: Tailoring Nanoarchitectures for Functional Applications. *Adv. Mater.* **2017**, *29*, 1700213.
(27) Yang, S.; Wang, Y.; Wu, X.; Sheng, S.; Wang, T.; Zan, X. Multifunctional Tannic Acid (TA) and Lysozyme (Lys) Films Built Layer by Layer for Potential Application on Implant Coating. *ACS Biomater. Sci. Eng.* **2019**, *5*, 3582−3594.
(28) Jiang, X.; He, S.; Han, G.; Long, J.; Li, S.; Lau, C. H.; Zhang, S.; Shao, L. Aqueous One-Step Modulation for Synthesizing Monodispersed ZIF-8 Nanocrystals for Mixed-Matrix Membrane. *ACS Appl. Mater. Interfaces* **2021**, *13*, 11296−11305.
(29) Hu, Y.; Kazemian, H.; Rohani, S.; Huang, Y.; Song, Y. In situ high pressure study of ZIF-8 by FTIR spectroscopy. *Chem. Commun.* **2011**, *47*, 12694−12696.
(30) Öztürk, Z.; Filez, M.; Weckhuysen, B. M. Decoding Nucleation and Growth of Zeolitic Imidazolate Framework Thin Films with Atomic Force Microscopy and Vibrational Spectroscopy. *Chem.—Eur. J.* **2017**, *23*, 10915−10924.
(31) Jiang, H.; Yan, Q.; Chen, R.; Xing, W. Synthesis of Pd@ZIF-8 via an assembly method: Influence of the molar ratios of Pd/Zn2+ and 2-methylimidazole/Zn2+. *Microporous Mesoporous Mater.* **2016**, *225*, 33−40.
(32) Lee, J. H.; Kim, D.; Shin, H.; Yoo, S. J.; Kwon, H. T.; Kim, J. Zeolitic imidazolate framework ZIF-8 films by ZnO to ZIF-8 conversion and their usage as seed layers for propylene-selective ZIF-8 membranes. *J. Ind. Eng. Chem.* **2019**, *72*, 374−379.
(33) Stock, N.; Biswas, S. Synthesis of Metal-Organic Frameworks (MOFs): Routes to Various MOF Topologies, Morphologies, and Composites. *Chem. Rev.* **2012**, *112*, 933−969.

https://doi.org/10.1021/acsomega.2c00939
ACS Omega 2022, 7, 17765−17773